J. Electr. Electron. Mater.
Vol. 38, No. 5, pp. 567-572 September 2025
doi: https://doi.org/10.4313/JEEM.2025.38.5.13
ISSN 1226-7945(Print), 2288-3258(Online)

Regular Paper

Development of a TEM-Integrated Cathodoluminescence Detection System for High-Resolution Optical Analysis of InGaN/GaN Quantum Well Structure

Sung-Dae Kim

Department of Materials Science and Engineering, Pukyong National University, Busan 48513, Korea

(Received July 15, 2025; Revised July 24, 2025; Accepted July 30, 2025)

Abstract: Cathodoluminescence (CL) spectroscopy provides valuable insights into the optical and electronic properties of materials by analyzing photon emission induced by electron beam excitation. In this study, we present a novel CL detection system integrated into a transmission electron microscope (TEM) specimen stage, enabling high-resolution optical analysis of internal microstructures. The system features a parabolic mirror, a focusing lens, and a UV-VIS range optical fiber to maximize light collection and transmission efficiency, with performance further enhanced by a liquid nitrogen cooling setup. Using this system, we successfully performed CL mapping of InGaN/GaN multiple quantum wells (MQWs) and GaN thin films. The results revealed that threading dislocations act as non-radiative centers in GaN and locally increase the bandgap energy in InGaN MQWs, causing a blue-shift in CL emission. These findings support a model in which dislocations induce carrier delocalization, preserving high radiative efficiency despite high dislocation densities. This work demonstrates the effectiveness of the TEM-integrated CL system for nanoscale optical characterization, offering a new pathway for studying defect-related phenomena in semiconductor materials.

Keywords: Cathodoluminescence, Transmission electron microscopy, Electron excitation, GaN, Light emitting diode

1. INTRODUCTION

As accelerated electron beams interact with materials, various signals are emitted that contain valuable structural, chemical, and electrical information. Electron microscopy leverages these signals to investigate and characterize materials at the micro- and nanoscale. Among these techniques, cathodoluminescence (CL) is the emission of photons induced by electron beam excitation. When high-energy primary electrons penetrate a material, they lose energy by generating electron-hole pairs. These carriers can recombine either radiatively, emitting photons in the ultraviolet (UV), visible, or infrared (IR) regions, or non-radiatively, without photon emission [1, 2].

The energy transfer from the incident electrons promotes electrons from the valence band into the conduction band, leaving behind positively charged holes [1-3]. These excited electrons and holes may migrate independently within their respective bands until recombination occurs. In the case of radiative recombination, the energy released corresponds to the photon energy of the emitted light, which reflects the material's bandgap structure. Consequently, cathodoluminescence spectroscopy provides insight into both intrinsic bandgap energies and extrinsic energy states within the bandgap [1-3].

CL analysis is typically conducted using a focused electron beam as the excitation source. The electron beam, composed

✉ **Sung-Dae Kim; sdkim@pknu.ac.kr**

of negatively charged particles, can be finely focused using electromagnetic lenses to sub-nanometer spot sizes. By scanning this focused beam over a region of interest, both the CL spectra and the microstructural information can be simultaneously obtained. Due to these capabilities, scanning electron microscopes (SEMs) are commonly employed for CL analysis [4-7]. SEMs offer a spacious specimen chamber, which facilitates the integration of optical components such as mirrors, lenses, and light guides required for efficient photon collection.

However, SEM-based CL primarily provides information limited to surface morphology [8-10]. Internal structural defects such as dislocations, stacking faults, and grain boundaries are difficult to detect using SEM. To address this limitation, a few research groups have explored CL analysis using transmission electron microscopes (TEMs), which offer superior spatial resolution and the ability to directly observe internal microstructures [11-13]. In these studies, custom-built CL detection systems were typically integrated into dedicated TEM columns, enabling detailed analysis of defect-related optical properties. Although these dedicated setups offer precise optical alignment, they are associated with significant challenges. The long optical path from the sample to the detector leads to substantial photon loss, and the integration of external optical systems within the TEM column raises concerns regarding vacuum compatibility and mechanical stability.

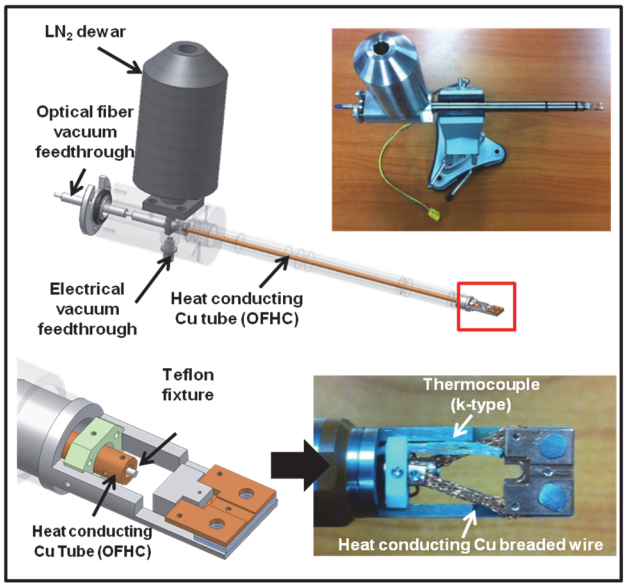

Fig. 1. A home-built TEM-CL detection system.

In this study, we developed a novel CL detection system compatible with conventional TEMs. Specifically, we designed a light-collecting TEM specimen stage (Fig. 1).

This system incorporates a carefully engineered assembly of optical components—including a parabolic mirror, focusing lens, and optical fiber—integrated within the specimen stage itself (Fig. 2). The spherical parabolic mirror surrounds the specimen and maximizes the photon collection angle. Light reflected from the mirror is focused by the lens and then guided through an optical fiber to a spectrometer, thereby minimizing optical losses during transmission. Additionally, a specimen cooling system was integrated into the stage. Cooling enhances CL emission intensity and enables more detailed spectral analysis by reducing thermal broadening and non-radiative recombination.

To evaluate the performance of the TEM-CL specimen stage, we detected the CL emission from InGaN/GaN quantu m well structure. This work demonstrates the effectiveness of our system in capturing localized optical signals from internal microstructures, offering a new pathway for high-resolution CL analysis within a standard TEM platform.

2. MATERIALS AND METHODS

Figure 2 illustrates the schematic design of the cathodoluminescence (CL) light collection process using the custom-designed TEM specimen stage. When an electron beam irradiates the specimen, CL signals—photons—are emitted isotropically. The parabolic mirror surrounding the specimen redirects the emitted light into collimated beams aligned with the optical axis of a focusing lens. A biconvex lens then focuses

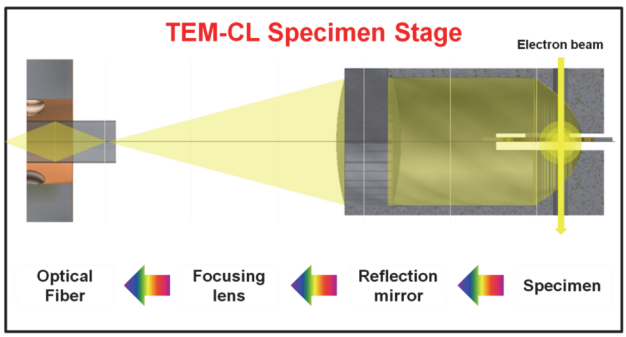

Fig. 2. Schematic image showing the operating principle of the TEM-CL detection system (cross-sectional view of the TEM-CL holder).

this parallel light onto its focal point, where the entrance facet of an optical fiber is precisely positioned to collect the focused light. The collected photons are subsequently transmitted to a spectrometer through the optical fiber.

A central component of the system is the parabolic mirror, designed to maximize light collection efficiency. Among various candidate materials, aluminum (Al) was selected due to its high reflectivity across the visible spectrum. The mirror's reflective surface was fabricated according to a standard parabolic equation with a focal length of 0.5 mm, positioning the specimen—where CL is generated—at the mirror's focal point to optimize parallelization of the emitted light. To focus the collimated light, a 3 mm-diameter fused silica biconvex lens was employed. The focal length of the lens was carefully selected based on the numerical aperture (NA) of the optical fiber and the critical angle for total internal reflection. A high-OH silica-core optical fiber, optimized for ultraviolet (UV) to visible (VIS) wavelengths, was used. The fiber has a 1 mm core diameter, which enhances light throughput. The fiber is coated with an acrylate buffer layer and an aluminum (Al) protective layer, providing both mechanical robustness and thermal protection during cryogenic operations.

The optical fiber used in this system has a numerical aperture (NA) of 0.22, corresponding to a maximum acceptance half-angle (θ_{max}) of 12.7° in air or vacuum, or approximately a 25° full acceptance cone. With the focal length of the focusing lens set to 6 mm, the majority of the focused rays fall within this acceptance angle, ensuring efficient light collection through total internal reflection.

Spectroscopic measurements were carried out using a QE65000 spectrometer (Ocean Optics), a compact, factory-aligned system with an integrated CCD detector. The spectrometer features a symmetrical crossed Czerny–Turner optical bench with a focal length of 101.6 mm and a 200 μm entrance slit. A grating with a groove density of 600 lines/mm and a blaze wavelength of 400 nm was employed. The groove density influences spectral dispersion and resolution, while the blaze angle optimizes efficiency in the desired spectral region. With the selected grating and slit configuration, the system achieves a spectral resolution of 3.13 nm at 400 nm. For photon detection, a Hamamatsu S7031-1006 back-thinned CCD was used, featuring a 1024 × 58 pixel array with 24 μm² pixel size, a well depth of 300,000 electrons/pixel, and quantum efficiency (QE) of 90% at 400 nm (and 65% at 250 nm). The system exhibits a conversion gain of 22 electrons/count, offering high sensitivity for low-light applications.

To further enhance CL signal intensity and spectral resolution, a liquid nitrogen (LN_2) cooling system was integrated into the TEM-CL specimen stage. A 200 mL LN_2 dewar was attached to the stage holder, connected via an oxygen-free high-conductivity copper (OFHC) tube. The optical fiber was routed through the inner channel of this tube. The tube was secured at the specimen stage tip using a Teflon block to thermally isolate the cooled region from the rest of the TEM structure and minimize heat conduction.

CL experiments were performed using a transmission electron microscope (JEOL 2010F) operated at an accelerating voltage of 120 keV. A 2D hyperspectral CL data set was obtained by scanning the electron beam over the region of interest using an external scanning unit (Oxford Instruments SEMI-STEM). GaN TEM samples were prepared through mechanical polishing, followed by argon ion milling at 3.5 kV using a Gatan PIPS system.

InGaN/GaN QW samples were prepared by conventional low pressure metal-organic chemical vapor deposition (MOCVD) method. The sample consists of a 3 mm-thick GaN layer grown on (0001) sapphire substrate and three period InGaN (3 nm)/GaN (20 nm) multiple quantum wells (MQWs) capped with a 150 nm-thick GaN layer. Trimethylgallium (TMGa), trimethylindium (TMIn) and ammonia (NH3) were used as Ga, In and N sources and hydrogen as carrier gas. Growth temperature of the InGaN and GaN layer is 740°C and 1040°C, respectively.

3. RESULTS AND EXPERIMENTAL VERIFICATION

Sapphire, the most commonly used substrate for GaN epitaxial growth, exhibits excellent thermal, chemical, and mechanical stability. However, sapphire possesses a corundum crystal structure, which is fundamentally different from the wurtzite structure of III-nitride semiconductors. Additionally, the lattice mismatch between sapphire and GaN results in a high density of misfit dislocations, typically on the order of 10^8–10^9 cm^{-2} [14].

Figure 3 presents a room temperature cathodoluminescence (CL) spectrum of a GaN thin film, featuring two prominent emission peaks: the band-edge emission at 364 nm and a broad

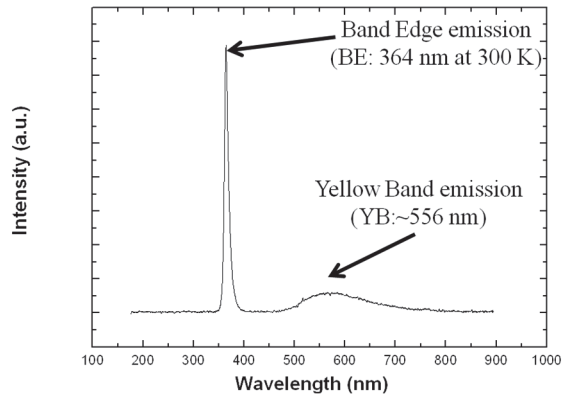

Fig. 3. Cathodoluminescence (CL) spectrum of a GaN thin film at room temperature.

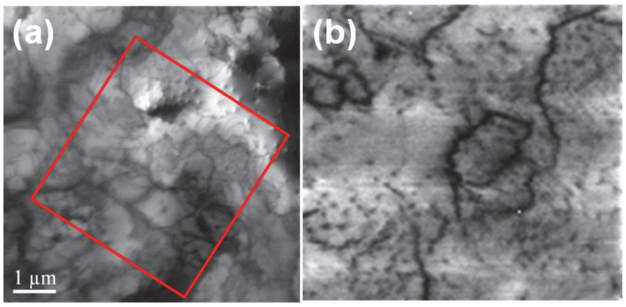

Fig. 4. (a) Plan-view bright-field TEM image and (b) monochromatic band-edge CL spectral image.

yellow luminescence band spanning 500 to 650 nm. The band-edge emission arises from band-to-band recombination of excited electrons, whereas the yellow band emission is attributed to defect-related states within the bandgap.

Plan-view transmission electron microscopy (TEM) and monochromatic band-edge CL spectral imaging (Figs. 4(a) and (b), respectively), performed on the region indicated by the red square, reveal that threading dislocations appear as dark spots in the CL images. This confirms that threading dislocations act as non-radiative recombination centers, quenching the band-edge emission in GaN films [1,3,14]. Moreover, a grain-like contrast observed in the CL images corresponds to arrangements of dislocations forming low-angle grain boundaries, as shown in Fig. 4. These low-angle grain boundaries originate from the low-temperature GaN buffer layer commonly deposited prior to the high-temperature GaN growth, and they degrade the band-edge emission.

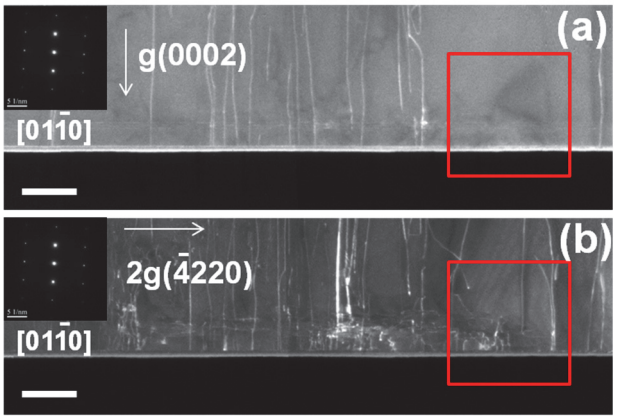

Fig. 5. Weak beam dark field images of a cross-sectional TEM specimen of the InGaN/GaN multiple quantum wells structure with two beam condition of (a) g (0002) and (b) 2g (-4220), respectively.

Despite these detrimental effects of dislocations, III-nitride materials, especially InGaN/GaN blue emitters, exhibit surprisingly high radiative efficiencies even at high dislocation densities [7-9,13]. This defect-insensitive luminescence behavior has been widely attributed to compositional alloy fluctuations, clustering, and phase separation in ternary and quaternary alloys such as InGaN and AlInGaN. These phenomena create local potential minima that spatially confine carriers, thereby preventing their diffusion towards non-radiative dislocation sites [11-17]. However, direct microstructural evidence supporting such localized potential minima remains elusive, and this explanation does not clarify how dislocations influence the bandgap structure of InGaN or AlInGaN alloys.

It has been reported [16] that that in the vicinity of V-shaped defects associated with dislocations, InGaN quantum wells become thinner, resulting in higher local bandgap energies that effectively shield dislocation cores from mobile carriers in thicker regions of the quantum wells. This mechanism could explain the maintenance of high radiative efficiency despite dislocations, although a direct correlation between well thickness variation and bandgap modulation has not been definitively demonstrated.

To further elucidate the influence of threading dislocations on the optical properties of InGaN/GaN multiple quantum wells (MQWs), we performed cross-sectional annular dark-field (ADF) scanning transmission electron microscopy (STEM) imaging alongside spatially resolved CL spectroscopy. Due to the reduced diffraction contrast in STEM, the

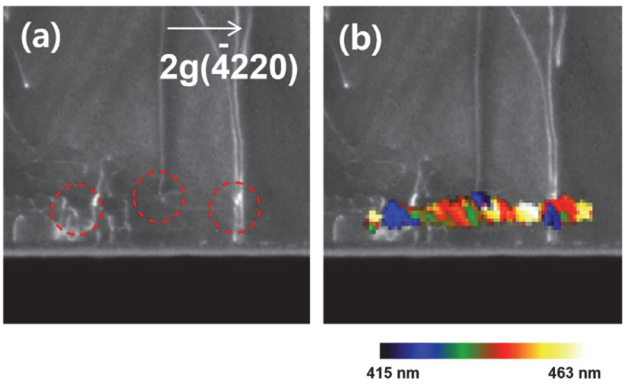

Fig. 6. (a) Cross-sectional weak beam dark field image of InGaN/GaN MQW structure and (b) overlapped image of the peak wavelength map of InGaN layer on (a).

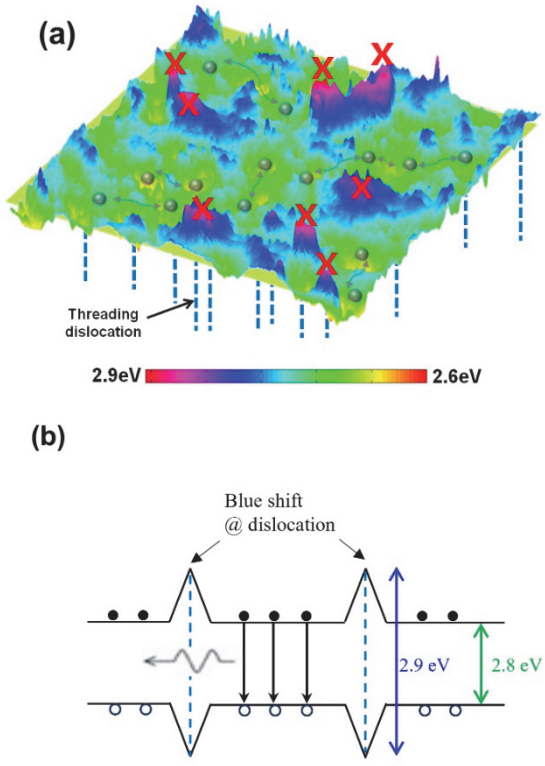

Fig. 7. (a) Schematic diagram of carrier delocalization in the region penetrated by dislocations and (b) schematic energy band diagram illustrating the redistribution of carriers.

precise locations of threading dislocations are clearly identifiable, facilitating direct correlation with CL emission properties.

To further clarify the relationship between dislocations and the peak wavelength shift, cross-sectional TEM specimens were analyzed under weak-beam dark field conditions with diffraction vectors g (0002) and 2g (-4220), as shown in Figs. 5(a) and (b). Most dislocations traverse the InGaN active layers. CL emission was collected from the square-marked regions, and Fig. 6 presents an overlapped image of the CL peak wavelength map on the weak-beam dark field TEM image. Regions penetrated by dislocations consistently exhibit a blue-shift in CL peak wavelength.

Consequently, it is evident that the observed blue-shift in the CL emission from InGaN active layers originates from threading dislocations. Based on these results, we propose a model where the defect insensitivity of radiative recombination in InGaN is attributed to the delocalization of carriers in regions affected by threading dislocations (Fig. 7). Threading dislocations locally increase the bandgap energy within the InGaN layers, creating energy barriers that repel carriers from the dislocation cores. As a result, carriers preferentially recombine radiatively in regions of lower bandgap energy, effectively maintaining high radiative efficiency despite high dislocation densities.

4. CONCLUSIONS

This study presents the development and application of a novel cathodoluminescence (CL) detection system integrated into a transmission electron microscope (TEM) specimen stage, enabling detailed optical analysis of internal microstructures in materials. The system incorporates a parabolic mirror, focusing lens, and UV-VIS range optical fiber to efficiently collect and transmit emitted light to a spectrometer, with enhanced performance via liquid nitrogen cooling. To evaluate the performance of this system, CL mapping of GaN material was performed. The CL map of GaN revealed that dislocations cause a blue-shift in emission wavelength, indicating increased bandgap energy at dislocated regions.

ORCID
Sung-Dae Kim https://orcid.org/0000-0003-4006-6111

ACKNOWLEDGMENTS

This work was supported by the Pukyong National University Research Fund in 2022 (202212380001).

REFERENCES

[1] B. G. Yacobi and D. B. Holt, *Cathodoluminescence Microscopy of Inorganic Solids*. (Springer Science & Business Media, 2013). doi: https://doi.org/10.1007/978-1-4757-9595-0

[2] N. Yamamoto, K. Araya, and F. J. García de Abajo, *Phys. Rev. B*, **64**, 205419 (2001). doi: https://doi.org/10.1103/PhysRevB.64.205419

[3] N. Yamamoto, *Cathodoluminescence* (InTech, 2012). doi: https://doi.org/10.5772/1989

[4] S. D. Kim, *J. Electr. Electron. Mater.*, **36**, 326 (2023). doi: https://doi.org/10.4313/JKEM.2023.36.4.2

[5] M. Kociak and L. F. Zagonel, *Ultramicroscopy*, **176**, 112 (2017). doi: https://doi.org/10.1016/j.ultramic.2017.03.014

[6] L. F. Zagonel, L. Rigutti, M. Tchernycheva, G. Jacopin, R. Songmuang, and M. Kociak, *Nanotechnology*, **23**, 455205 (2012). doi: https://doi.org/10.1088/0957-4484/23/45/455205

[7] L. F. Zagonel, S. Mazzucco, M. Tence, K. March, R. Bernard, B. Laslier, G. Jacopin, M. Tchernycheva, L. Rigutti, F. H. Julien, R. Songmuang, and M. Kociak, *Nano Lett.*, **11**, 568 (2011). doi: https://doi.org/10.1021/nl103549t

[8] F. J. García de Abajo, *Rev. Mod. Phys.*, **82**, 209 (2010). doi: https://doi.org/10.1103/RevModPhys.82.209

[9] S. Meuret, L. H. G. Tizei, T. Auzelle, R. Songmuang, B. Daudin, B. Gayral, and M. Kociak, *ACS Photonics*, **3**, 1157 (2016). doi: https://doi.org/10.1021/acsphotonics.6b00212

[10] A. Losquin, L. F. Zagonel, V. Myroshnychenko, B. Rodríguez-González, M. Tencé, L. Scarabelli, J. Förstner, L. M. Liz-Marzán, F. J. García de Abajo, O. Stéphan, and M. Kociak, *Nano Lett.*, **15**, 1229 (2015). doi: https://doi.org/10.1021/nl5043775

[11] P. R. Edwards and R. W. Martin, *Semicond. Sci. Technol.*, **26**, 064005 (2011). doi: https://doi.org/10.1088/0268-1242/26/6/064005

[12] O. L. Krivanek, T. C. Lovejoy, N. Dellby, T. Aoki, R. W. Carpenter, P. Rez, E. Soignard, J. Zhu, P. E. Batson, M. J. Lagos, R. F. Egerton, and P. A. Crozier, *Nature*, **514**, 209 (2014). doi: https://doi.org/10.1038/nature13870

[13] Z. Mahfoud, A. T. Dijksman, C. Javaux, P. Bassoul, A. L. Baudrion, J. Plain, B. Dubertret, and M. Kociak, *J. Phys. Chem. Lett.*, **4**, 4090 (2013). doi: https://doi.org/10.1021/jz402233x

[14] R. Gómez-Medina, N. Yamamoto, M. Nakano, and F. J. García de Abajo, *New J. Phys.*, **10**, 105009 (2008). doi: https://doi.org/10.1088/1367-2630/10/10/105009

[15] S. T. Kim and D. C. Moon, *J. Korean Inst. Electr. Electron. Mater. Eng.*, **11**, 784 (1998).

[16] J. M. Lee, W. Son, J. Kim, J. H. Noh, M. Oh, J. H. Choi, and C. Choi, *J. Korean Inst. Electr. Electron. Mater. Eng.*, **36**, 303 (2023). doi: https://doi.org/10.4313/JKEM.2023.36.4.1

[17] M. Grundmann, J. Christen, N. N. Ledentsov, J. Böhrer, D. Bimberg, S. Ruvimov, P. Werner, U. Richter, U. Gösele, J. Heydenreich, V. M. Ustinov, A. Y. Egorov, A. E. Zhukov, P. S. Kop'ev, and Z. I. Alferov, *Phys. Rev. Lett.*, **74**, 4043 (1995). doi: https://doi.org/10.1103/PhysRevLett.74.4043